Plasma Chem Plasma Process (2007) 27:267–291
DOI 10.1007/s11090-007-9053-7

ORIGINAL PAPER

Thermodynamic and Transport Properties of Two-temperature Oxygen Plasmas

S. Ghorui · Joachim V. R. Heberlein · E. Pfender

Published online: 14 April 2007
© Springer Science+Business Media, LLC 2007

Abstract Thermodynamic and transport properties of two-temperature oxygen plasmas are presented. Variation of species densities, mass densities, specific heat, enthalpy, viscosity, thermal conductivity, collision frequency and electrical conductivity as a function of temperature, pressure and different degree of temperature non-equilibrium are computed. Reactional, electronic and heavy particle components of the total thermal conductivity are discussed. To meet practical needs of fluid-dynamic simulations, temperatures included in the computation range from 300 K to 45,000 K, the ratio of electron temperature (T_e) to the heavy particle temperature (T_h) ranges from 1 to 30 and the pressure ranges from 0.1 to 7 atmospheres. Results obtained for thermodynamic equilibrium ($T_e = T_h$) under atmospheric pressure are compared with published results obtained for similar conditions. Observed overall agreement is reasonable. Slight deviations in some properties may be attributed to the values used for collision integral data and for the two temperature formulations used. An approach for computing properties under chemical non-equilibrium and associated deviations from two-temperature results under similar conditions are discussed.

Keywords Non-equilibrium thermodynamic and transport properties · oxygen plasmas

S. Ghorui · J. V. R. Heberlein · E. Pfender
Department of Mechanical Engineering, University of Minnesota,
Minneapolis, MN 55455, USA

S. Ghorui (✉)
Laser and Plasma Technology Division, Bhabha Atomic Research Centre,
Trombay, Mumbai 400 085, India
e-mail: srikumarghorui@yahoo.com

Introduction

Oxygen as plasma gas in plasma cutting torches offers higher quality surfaces inside the kerf, better removal of molten metal, less dross formation beneath the work piece and faster cutting speed. To meet the industrial requirements of precision, cost, quality and quantity and to compete with existing technologies, new developments consider smaller nozzle diameters, higher currents and higher flow rate of gases. Enormous constriction of the arc (nozzle diameter $\sim$2 mm), extremely high temperatures (> 30,000 K) at the core, extremely sharp gradient of temperature ($\geq 10^4$ K/mm) and associated high flow fields ($M > 1$) promote in these new generation of plasma torches significant deviations from thermal and chemical equilibrium. While, optimum designs of such plasma devices definitely require a thorough understanding of the impact of device design parameters on the ultimate fluid dynamic and electromagnetic characteristics, availability of non-equilibrium properties of oxygen plasma is a prerequisite. This paper addresses this issue and offers a complete study on the non-equilibrium transport and thermodynamic properties of oxygen plasmas necessary for such investigations.

Transport properties of thermal plasmas have been extensively studied [1–8] for various pure as well as binary mixtures of plasma gases under local thermal equilibrium (LTE) conditions, based on the solution of the Boltzmann equation using the Chapman-Enskog's [9–10] approach. Assuming a complete decoupling between electrons and heavy particles, Devoto [11, 12] and later Miller [13], Kannappan [14] and Bonnefoi [15] have derived transport coefficients of two temperature plasmas. Aubreton et al. [16] have reported two-temperature transport properties of Ar–O_2 plasmas under atmospheric pressure. Recently, it has been shown by Rat et al. [17, 18] that due to the assumption of complete decoupling between electrons and heavy particles, values of diffusion coefficients used by Devoto in earlier computations were not consistent with mass conservation. Afterward, two-temperature properties including diffusion have been reported by Rat et al. [19–21] for argon plasmas and by Aubreton et al. [22] for argon-helium plasmas.

While, most of the reported results are for atmospheric pressure and include temperature ranges below 30,000 K and $\theta(= T_e/T_h)$ values $\leq$ 10, no two-temperature properties are available for pure oxygen plasmas. Moreover, inside of such plasma torches, pressure can practically vary from several atmospheres to sub-atmospheric and there is increasing experimental evidence that temperature inside constricted nozzles ($\sim$2 mm dia), plasma temperatures at higher currents ($\sim$200 A) may well exceed 30,000 K. Also, near the wall, the non-equilibrium parameter θ can reach values beyond 20. Another reason for considering temperatures beyond 30,000 K is to achieve convergence in numerical simulations. It has been observed that even though the maximum temperature in a final converged solution may not exceed 30,000 K, it may easily exceed this limit at some intermediate stages of the computation. Unavailability of property data, physically compatible with the associated temperature variation, often leads to divergence of the code.

In this paper we have presented a complete set of thermodynamic and transport properties as required for numerical simulation of non-equilibrium oxygen plasmas at higher currents. Necessary collision integral values for computations are either collected from the literature or calculated. Cases, where integral values are available only for lower ranges of temperature, data have been extrapolated based on the available data. To take proper account of multicomponent diffusion and thermal diffusion in multi-temperature plasmas, results from the study of Ramshaw [23, 24] have been used. Under chemical non-equilibrium, number

densities inside the plasma are influenced by diffusive particle fluxes originating from species and temperature gradients. The ultimate effect can be accounted for by including a modified rate constant in the associated rate equations in place of chemical-equilibrium rate constants. A chemical non-equilibrium parameter 'r' is defined as the ratio of the modified rate constant to the equilibrium rate constant. Based on practical needs, ranges of pressure, temperature and θ are selected to vary respectively from 0.1 atm to 7 atm, 300 K to 45,000 K and from 1 to 30.

Details of the computational approach are presented in Section 'Method used for determination of thermodynamic properties of two temperatur oxygen plasmas'. For $\theta = r = 1$ results correspond to chemical as well as thermal equilibrium. Properties are available from previously published reports [3] and can be readily compared for this case. Such comparisons are presented in Section 'Method used for determination of transport properties of two temperature oxygen plasmas' together with other major results obtained from the study. Conclusions are presented in Section 'Results'.

Method Used for Determination of Thermodynamic Properties of two Temperature Oxygen Plasmas

Computation starts with the assumption that independent, simultaneous chemical reactions, taking place inside the oxygen plasma under a given pressure, are as follows:

(1) $O_2 = O + O$
(2) $O^+ = O - e$
(3) $O^{++} = O^+ - e$

Total number of species in the system is therefore five: molecule (M), atom (A), single ion (I), double ion (D) and electron(e). It is assumed that the populations of excited levels inside the atoms and the ions are governed by the electron temperature(T_e) while that of the rotational-vibrational levels of molecules are governed by the heavy particle temperatures (T_h). In the system all the electrons follow a temperature T_e and all other particles except electrons follow a temperature T_h. The total partition function of a species 'i' is the product of its internal (Q^i_{int}) and translational partition functions (Q^i_{tr}). The internal partition function is a product of rotational (Q^i_{rot}), vibrational(Q^i_{vib}), electronic (Q^i_{el}) and nuclear partition functions. Contributions from nuclear partition functions are neglected in the formulation since the nuclei play no part in associated chemical processes. Under this assumption, the internal and translational partition functions of involved species are listed in Table 1. Q^i_{int}, Q^i_{tr}, Q^i_{rot}, and Q^i_{vib} respectively present internal, translational, rotational

Table 1 Internal and translational partition functions for the used model

Species	Internal partition function	Translational partition function [V = volume of system]
M	$Q^M_{int} = Q^M_{rot} \cdot Q^M_{vib}$	$Q^M_{tr} = V \cdot \left(\frac{2\pi m_M k_B T_h}{h^2}\right)^{3/2}$
A	$Q^A_{int} = Q^A_{el}$	$Q^A_{tr} = V \cdot \left(\frac{2\pi m_A k_B T_h}{h^2}\right)^{3/2}$
I	$Q^I_{int} = Q^I_{el}$	$Q^I_{tr} = V \cdot \left(\frac{2\pi m_I k_B T_h}{h^2}\right)^{3/2}$
D	$Q^D_{int} = Q^D_{el}$	$Q^D_{tr} = V \cdot \left(\frac{2\pi m_D k_B T_h}{h^2}\right)^{3/2}$
e	$Q^e_{int} = 2$	$Q^e_{tr} = V \cdot \left(\frac{2\pi m_e k_B T_e}{h^2}\right)^{3/2}$

and vibrational partition function of species i. m_i, k_B and h respectively correspond to mass of species i, Boltzmann constant and Planck's constant.

Explicit forms of rotational, vibrational and electronic partition functions are presented in the following.

$$Q_{\mathrm{rot}}^{\mathrm{M}} = \frac{T_{\mathrm{h}}}{\Theta_{\mathrm{rot}}} \tag{1}$$

$$Q_{\mathrm{vib}}^{\mathrm{M}} = \exp\left(-\frac{\Theta_{\mathrm{vib}}}{2T_{\mathrm{h}}}\right) / \left[1 - \exp\left(-\frac{\Theta_{\mathrm{vib}}}{2T_{\mathrm{h}}}\right)\right] \tag{2}$$

$$Q_{\mathrm{el}}^{\mathrm{i}} = \sum_j g_{\mathrm{ij}} \exp\left(-\frac{E_{\mathrm{ij}}}{k_{\mathrm{B}} T_{\mathrm{e}}}\right) \tag{3}$$

Θ_{rot} and Θ_{vib} are respectively characteristic rotational temperature (=2.09 K for Oxygen) and vibrational temperature (=2,260 K for Oxygen). E_{ij} refers to the energy of jth electronic excited level of species i and g_{ij} corresponds to its degeneracy.

The appropriate method for determination of number density in a multi-temperature plasma has long been a subject of debate [25, 26]. In the present case we have used maximization of entropy [26, 27] that results in the set of Eqs. (4)–(6) which are subsequently solved together with Eq. (7) to obtain the number density of the species present in the plasma.

$$\frac{p_A^2}{p_{\mathrm{M}}} = \frac{k_{\mathrm{B}} T_{\mathrm{h}} \left\{ \left(\frac{2\pi m_{\mathrm{A}} k_{\mathrm{B}} T_{\mathrm{h}}}{h^2} \right)^{3/2} \right\}^2}{\left(\frac{2\pi m_{\mathrm{M}} k_{\mathrm{B}} T_{\mathrm{h}}}{h^2} \right)^{3/2}} \cdot \frac{\left\{ Q_{\mathrm{int}}^{\mathrm{A}}(T_{\mathrm{e}}) \right\}^2}{Q_{\mathrm{int}}^{\mathrm{M}}(T_{\mathrm{h}})} \cdot \exp\left[-\left\{ \frac{2E_{\mathrm{A}}}{k_{\mathrm{B}} T_{\mathrm{e}}} \right\} + \frac{E_{\mathrm{M}}}{k_{\mathrm{B}} T_{\mathrm{h}}} \right] \tag{4}$$

$$\frac{p_{\mathrm{e}} p_{\mathrm{I}}}{p_{\mathrm{A}}} = \frac{Q_{\mathrm{int}}^{\mathrm{I}}(T_{\mathrm{e}})}{Q_{\mathrm{int}}^{\mathrm{A}}(T_{\mathrm{e}})} \cdot \left(\frac{2\pi m_{\mathrm{e}} k_{\mathrm{B}} T_{\mathrm{e}}}{h^2} \right)^{3/2} \cdot (2k_{\mathrm{B}} T_{\mathrm{e}}) \cdot \exp\left(-\frac{E_{\mathrm{I}} - E_{\mathrm{A}}}{k_{\mathrm{B}} T_{\mathrm{e}}} \right) \tag{5}$$

$$\frac{p_{\mathrm{e}} p_{\mathrm{D}}}{p_{\mathrm{I}}} = \frac{Q_{\mathrm{int}}^{\mathrm{D}}(T_{\mathrm{e}})}{Q_{\mathrm{int}}^{\mathrm{I}}(T_{\mathrm{e}})} \cdot \left(\frac{2\pi m_{\mathrm{e}} k_{\mathrm{B}} T_{\mathrm{e}}}{h^2} \right)^{3/2} \cdot (2k_{\mathrm{B}} T_{\mathrm{e}}) \cdot \exp\left(-\frac{E_{\mathrm{D}} - E_{\mathrm{I}}}{k_{\mathrm{B}} T_{\mathrm{e}}} \right) \tag{6}$$

$$p = \sum n_{\mathrm{i}} k_{\mathrm{B}} T_{\mathrm{i}} \tag{7}$$

Appropriate values for E_{M}, E_{I} and E_{D} for oxygen plasma are respectively: 5.115 eV, 13.614 eV and 48.722 eV. $E_{\mathrm{I}}-E_{\mathrm{A}}$ presents the energy required for first ionization and so on. p is the total pressure in which p_{i} is the partial pressure of species i. Lowering of the ionization energy [28] due to the interaction of charged particles has been included in the final computation.

From the number densities, the specific internal energy of the system is computed from respective translational and internal partition functions as follows:

$$\varepsilon = \frac{1}{\rho} \sum_i \left[n_{\mathrm{i}} k_{\mathrm{B}} T_{\mathrm{i}}^2 \frac{\partial \ln Q_{\mathrm{tr}}^{\mathrm{i}}}{\partial T_{\mathrm{i}}} \right]_V + \frac{1}{\rho} \sum_i \left[n_{\mathrm{i}} k_{\mathrm{B}} T_{\mathrm{i}}^2 \frac{\partial \ln Q_{\mathrm{int}}^{\mathrm{i}}}{\partial T_{\mathrm{i}}} \right]_V \tag{8}$$

ρ is mass density. Thermodynamic properties are computed from internal energies employing standard thermodynamic relationships.

Method Used for Determination of Transport Properties of Two Temperature Oxygen Plasmas

For calculating transport properties, the distribution functions followed by the species in the plasma is assumed to be a first order perturbation to the Maxwellian distribution. The perturbation is then expressed in a series of Sonine polynomials [9], which finally through linearization of the Boltzmann equation leads to a system of linear equations that can be solved to obtain different transport coefficients [10, 29]. While the elements in the matrix of the system of equations depend on the interaction between associated colliding species in terms of collision integrals, the number of elements depends on the order of the chosen approximation. In the following we describe in brief the definition of collision integrals and prescription used for computing different transport properties from them.

Collision Integrals

The collision integrals for interaction between species i and j are defined as following [9, 10, 29, 30]:

$$\Omega_{\mathrm{ij}}^{(\mathrm{l,s})} = \left(\frac{kT_{\mathrm{ij}}^{*}}{2\pi m_{\mathrm{ij}}^{*}}\right)\int_{0}^{\infty} e^{-\gamma^2}\gamma^{2s+3}Q_{\mathrm{ij}}^{(l)}(g)d\gamma \tag{9}$$

where g is the relative speed between colliding particles, $Q_{\mathrm{ij}}^{(l)}(g)$ is the gas kinetic cross-section which is a function of impact parameter, deflection angle and associated interaction potential [9]. $\gamma^2 = m^{*}_{\mathrm{ij}}g^2/2k_{\mathrm{B}}T_{\mathrm{ij}}^{*}$ and m_{ij}^{*} and T_{ij}^{*} are the reduced mass and temperature i.e.:

$$m_{\mathrm{ij}}^{*} = \frac{m_{\mathrm{i}}m_{\mathrm{j}}}{(m_{\mathrm{i}}+m_{\mathrm{j}})}; T_{\mathrm{ij}}^{*} = \frac{m_{\mathrm{i}}T_{\mathrm{j}}+m_{\mathrm{j}}T_{\mathrm{i}}}{(m_{\mathrm{i}}+m_{\mathrm{j}})} \tag{10}$$

All properties except the electrical conductivity and the translational thermal conductivity of electrons have been computed considering up to the second-order approximation [30] for which one needs to consider only the integrals: $\Omega_{\mathrm{ij}}^{(1,1)}$, $\Omega_{\mathrm{ij}}^{(1,2)}$, $\Omega_{\mathrm{ij}}^{(1,3)}$ and $\Omega_{\mathrm{ij}}^{(2,2)}$. Collision integrals associated with $O^{+}-O_2$, $O^{++}-O_2$, and $O^{++}-O$ interactions are computed using polarization potentials following suggestions of Devoto [1]. The remaining integral values are available [31–34] in the literature in form of reduced integrals as listed in Table 2. However, covered ranges of temperature are somewhat limited in these

Table 2 Sources of collision integral data/formulation

Interaction	Method	Reference
O–O	Collision integral tabulation (CIT)	Levin [31]
O_2-O_2	CIT	Yun [32]
O_2-O	CIT	Yun [32]
$O^{+}-O_2$	Polarization potential	Devoto [1]
$O^{++}-O_2$	Polarization potential	Devoto [1]
$O^{+}-O$	CIT	Stallcop [33]
$O^{++}-O$	Polarization potential	Devoto [1]
e–O	CIT	Devoto [34]
e–O_2	CIT	Devoto [34]

references except for [31]. To cover the range of our interest (300K-45000K), available integral values are extrapolated based on the available data. For charged species, collision integrals are computed using screened Coulomb potentials according to Liboff [35]. Recursion formulae [32] have been used for derivation of $\Omega_{ij}^{(l,s+1)}$ integrals from $\Omega_{ij}^{(l,s)}$ integrals for O_2-O_2 and O_2-O interactions. For electron neutral interactions, following Murphy [3], it has been assumed that $\Omega_{ij}^{(l,s)} = \Omega_{ij}^{(1,1)}$.

Cross-sections are computed from respective integrals using the following relationship [9]:

$$Q_{ij}^{(l,s)} = \frac{\Omega_{ij}^{(l,s)}}{\frac{(s+1)!\left[2l+1-(-1)^l\right]}{4(l+1)}\sqrt{\frac{k_B T_{ij}^*}{2\pi m_{ij}^*}}} \tag{11}$$

Diffusion Coefficients

A total of 85 different diffusion coefficients are required for the calculation of transport properties in the present formulation for the number of species considered. Computation starts from binary diffusion coefficients and then the remaining diffusion coefficients are computed in terms of them. To take proper account of multi-component binary diffusion in a multi-temperature plasma, the formulation developed by Ramshaw [23, 24] has been used. The binary diffusion coefficient between two particles i and j for this diffusion model appears as:

$$D_{ij}^b = \frac{3k_B^2 T_i T_j}{16 p m_{ij}^* \Omega_{ij}^{(1,1)} \cdot T_{ij}^*} \tag{12}$$

Here, T_i and T_j are temperatures of ith and jth particle respectively. p is the pressure, $\Omega_{ij}^{(1,1)}$ is the collision integral and k_B is the Boltzmann constant. Reduced mass m_{ij}^* and reduced temperature T_{ij}^* are used as defined in (10). Once the temperatures are known, twenty five binary diffusion coefficients associated with this case are computed in this manner using already available $\Omega_{ij}^{(1,1)}$ values. Subsequently, all other diffusion coefficients are derived from these binary diffusion coefficients using standard relationships [9].

The first approximation to the general diffusion coefficients in terms of binary diffusion coefficients can be written as [9]:

$$D_{ij} = \frac{F^{ji} - F^{ii}}{m_j |F|} \tag{13}$$

where, F^{ij} is a cofactor of F_{ij}, defined in terms of binary diffusion coefficients as [9]:

$$F_{ij} = \frac{1}{\rho}\left[\frac{n_i}{D_{ij}^b} + \sum_{l \neq i} \frac{n_i m_j}{m_i D_{il}^b}\right]\left(1 - \delta_{ij}\right) \tag{14}$$

ρ, δ_{ij} and n_i correspond to mass density, Kronecker delta symbol and number density of species i. General ambipolar diffusion coefficients are defined in terms of general diffusion coefficients as following [36]:

$$D_{\mathrm{ij}}^{\mathrm{a}} = D_{\mathrm{ij}} + \frac{\alpha_{\mathrm{i}}}{\beta} \sum_{k} Z_{\mathrm{k}} D_{\mathrm{kj}} \tag{15}$$

where, α and β can be expressed in terms of charge, mass, number density, temperature and associated general diffusion coefficients of the participating particles as follows [37]:

$$\alpha_{\mathrm{i}} = \sum_{j} \frac{m_{\mathrm{j}} n_{\mathrm{j}} Z_{\mathrm{j}} D_{\mathrm{ij}}}{T_{\mathrm{j}}} \tag{16}$$

$$\beta = -\sum_{i} Z_{\mathrm{i}} \sum_{j} \frac{m_{\mathrm{j}} n_{\mathrm{j}} Z_{\mathrm{j}} D_{\mathrm{ij}}}{T_{\mathrm{j}}} \tag{17}$$

Z_{j} refer to the number of charges of species j. The total number of ambipolar diffusion coefficients and binary diffusion coefficients computed this way are twenty five each for this problem.

The thermal diffusion coefficients of electrons are computed using third approximation as [11]:

$$D_{\mathrm{e}}^{\mathrm{T}} = \frac{15 n_{\mathrm{e}}^2 \sqrt{2\pi m_{\mathrm{e}} k_B T_{\mathrm{e}}}}{4} \frac{\begin{vmatrix} q^{01} & q^{02} \\ q^{21} & q^{22} \end{vmatrix}}{\begin{vmatrix} q^{00} & q^{01} & q^{02} \\ q^{10} & q^{11} & q^{12} \\ q^{20} & q^{21} & q^{22} \end{vmatrix}} \tag{18}$$

expressions given by Devoto [11] for various q^{ij} elements in terms of cross-sections, $Q_{\mathrm{ij}}^{(\mathrm{l,s})}$, have been used in the computation.

Five thermal diffusion coefficients of heavy particles are computed using second approximation as [11]:

$$D_{\mathrm{i}}^{\mathrm{T}} = \frac{15 n_{\mathrm{e}}^2 \sqrt{2\pi m_{\mathrm{e}} k_{\mathrm{B}} T_{\mathrm{e}}}}{4} \frac{\begin{vmatrix} q_{\mathrm{jk}}^{00} & q_{\mathrm{jk}}^{01} & 0 \\ q_{\mathrm{jk}}^{10} & q_{\mathrm{jk}}^{11} & n_{\mathrm{j}} \\ \delta_{\mathrm{ki}} & 0 & 0 \end{vmatrix}}{\begin{vmatrix} q_{\mathrm{jk}}^{00} & q_{\mathrm{jk}}^{01} \\ q_{\mathrm{jk}}^{10} & q_{\mathrm{jk}}^{11} \end{vmatrix}} \tag{19}$$

Each $q_{\mathrm{ij}}^{\mathrm{mp}}$ block actually presents an array as following:

$$q_{\mathrm{ij}}^{\mathrm{mp}} = \begin{matrix} q_{11}^{\mathrm{mp}} & \cdots & q_{iv}^{\mathrm{mp}} \\ \vdots & & \vdots \\ q_{v1}^{\mathrm{mp}} & \cdots & q_{vv}^{\mathrm{mp}} \end{matrix} \tag{20}$$

v is the number of species in the system. Sixty four $q_{\mathrm{ij}}^{(\mathrm{l,s})}$ elements, necessary to evaluate the above determinant have been computed according to Devoto[30].

Five ambipolar thermal diffusion coefficients are computed from respective thermal diffusion coefficients and general diffusion coefficients as [36]:

$$D_{\mathrm{i}}^{\mathrm{Ta}} = D_{\mathrm{i}}^{\mathrm{T}} + \frac{m_{\mathrm{i}}\alpha_{\mathrm{i}}}{\beta}\sum_{\mathrm{j}} Z_{\mathrm{j}}\frac{D_{\mathrm{j}}^{\mathrm{T}}}{m_{\mathrm{k}}} \tag{21}$$

Thermal Conductivity of Electrons

Using the elements computed for diffusion coefficients of electrons, the translational thermal conductivity of electrons in the third approximation is computed as [11]:

$$k_{\mathrm{tr,e}} = \frac{75 n_{\mathrm{e}}^2 k_{\mathrm{B}}}{8}\left(\frac{2\pi k_{\mathrm{B}} T_{\mathrm{e}}}{m_{\mathrm{e}}}\right)^{1/2}\frac{1}{q^{11} - \frac{(q_{12})^2}{q^{22}}} \tag{22}$$

Thermal Conductivity of Heavy Particles

Using elements used in heavy particle diffusion coefficients, the translational thermal conductivity of heavy particles is computed as [30]:

$$k_{\mathrm{tr,h}} = -\frac{75 k_{\mathrm{B}}}{8}\frac{\sqrt{2\pi k_{\mathrm{B}} T_{\mathrm{h}}}}{|q|}\begin{vmatrix} q_{\mathrm{ij}}^{00} & q_{\mathrm{ij}}^{01} & 0 \\ q_{\mathrm{ij}}^{10} & q_{\mathrm{ij}}^{11} & n_{\mathrm{i}} \\ 0 & n_{\mathrm{j}}/\sqrt{m_{\mathrm{j}}} & 0 \end{vmatrix} \tag{23}$$

Electrical Conductivity

The electrical conductivity is computed in the third approximation using the q^{ij} elements as obtained in the diffusion expressions as follows [11]:

$$\sigma = \left(\frac{e^2 n m_{\mathrm{e}} n_{\mathrm{e}}}{\rho k_{\mathrm{B}} T_{\mathrm{e}}}\right)\cdot\left(\frac{3 n_{\mathrm{e}}\rho}{2 n m_{\mathrm{e}}}\right)\cdot\sqrt{\frac{2\pi k_{\mathrm{B}} T_{\mathrm{e}}}{m_{\mathrm{e}}}}\begin{vmatrix} q^{11} & q^{12} \\ q^{21} & q^{22} \end{vmatrix} \Big/ \begin{vmatrix} q^{00} & q^{01} & q^{02} \\ q^{10} & q^{11} & q^{12} \\ q^{20} & q^{21} & q^{22} \end{vmatrix} \tag{24}$$

Viscosity

Viscosity is a property of heavy particles only and therefore for oxygen plasma involves only O_2, O, O^+ and O^{++}. In this study viscosity is computed using first approximation as follows [30]:

$$\mu = -\frac{5\sqrt{2\pi k_B T_h}}{2} \frac{\begin{vmatrix} \hat{q}^{00}_{MM} & \hat{q}^{00}_{MA} & \hat{q}^{00}_{MI} & \hat{q}^{00}_{MD} & n_M\sqrt{m_M} \\ \hat{q}^{00}_{AM} & \hat{q}^{00}_{AA} & \hat{q}^{00}_{AI} & \hat{q}^{00}_{AD} & n_A\sqrt{m_A} \\ \hat{q}^{00}_{IM} & \hat{q}^{00}_{IA} & \hat{q}^{00}_{II} & \hat{q}^{00}_{ID} & n_I\sqrt{m_I} \\ \hat{q}^{00}_{DM} & \hat{q}^{00}_{DA} & \hat{q}^{00}_{DI} & \hat{q}^{00}_{DD} & n_D\sqrt{m_D} \\ n_M & n_A & n_I & n_D & 0 \end{vmatrix}}{\begin{vmatrix} \hat{q}^{00}_{MM} & \hat{q}^{00}_{MA} & \hat{q}^{00}_{MI} & \hat{q}^{00}_{MD} \\ \hat{q}^{00}_{AM} & \hat{q}^{00}_{AA} & \hat{q}^{00}_{AI} & \hat{q}^{00}_{AD} \\ \hat{q}^{00}_{IM} & \hat{q}^{00}_{IA} & \hat{q}^{00}_{II} & \hat{q}^{00}_{ID} \\ \hat{q}^{00}_{DM} & \hat{q}^{00}_{DA} & \hat{q}^{00}_{DI} & \hat{q}^{00}_{DD} \end{vmatrix}} \tag{25}$$

Associated elements of interest are computed in terms of cross-sections as [30]:

$$\hat{q}^{00}_{ij} = 8n_i\left(\frac{m_i}{m_j}\right)\sum_l \frac{n_l\sqrt{m_l}}{(m_i+m_l)^{3/2}}\left[\frac{10}{3}Q^{(1,1)}_{il}(\delta_{ij}-\delta_{jl})m_j + 2m_l Q^{(2,2)}_{il}(\delta_{ij}+\delta_{jl})\right] \tag{26}$$

Reactive Thermal Conductivity of Electrons and Heavy Particles

A formulation originally developed by Bose [38] has been used for computation of reactive thermal conductivities. In a multi-species control volume having particle density gradients $\nabla\, p_j$ for species j, the particle flux vector of species s is given by:

$$\Psi_s = \frac{n}{\rho k_B T_s}\sum_j \frac{T_s}{T_j} m_j D^a_{sj}\nabla p_j \tag{27}$$

The heat flux associated with the particle flux according to the independent reactions (1)–(3), can be written as:

$$\vec{q}_R = \Delta h_1 \cdot \vec{\Psi}_M + \Delta h_2 \cdot \vec{\Psi}_I + \Delta h_3 \cdot \vec{\Psi}_D \tag{28}$$

where Δ h_1, Δ h_2 and Δ h_3 are respectively the heat of reactions specified in Eqs. (1), (2) and (3) and can be estimated as;

$$\Delta h_1 = \frac{3}{2}k_B T_h + 2k_B T_e^2 \frac{\partial \ln Q^A_{int}}{\partial T_e} - k_B\Theta_{vib}\left(\frac{1}{2}+\exp\left(-\frac{\Theta_{vib}}{T_h}\right)\right) + E_d \tag{29}$$

$$\Delta h_2 = -\frac{5}{2}k_B T_e + k_B T_e^2 \frac{\partial \ln Q^A_{int}}{\partial T_e} - k_B T_e^2 \frac{\partial \ln Q^I_{int}}{\partial T_e} - E_1 \tag{30}$$

$$\Delta h_3 = -5k_B T_e + k_B T_e^2 \frac{\partial \ln Q^A_{int}}{\partial T_e} - k_B T_e^2 \frac{\partial \ln Q^D_{int}}{\partial T_e} - (E_1 + E_2) \tag{31}$$

E_d, E_1 and E_2 are respectively, dissociation, first and second ionization energies. Q_{int} refers to the internal partition function. Θ_{rot} and Θ_{vib} are respectively characteristic rotational (=2.09 K for O_2) and vibrational (=2,260 K for O_2) temperatures.

After substitution, Eq. (28) can be equivalently written as:

$$q_{\mathrm{R}} = \sum_{s=1}^{\mu} h_{\mathrm{s}} \vec{\psi}_{\mathrm{s}} = -k_{\mathrm{re}} \nabla T_{\mathrm{e}} - k_{\mathrm{rh}} \nabla T_{\mathrm{h}} \tag{32}$$

where,

$$\begin{aligned} k_{\mathrm{re}} = & \frac{n}{\rho k_{\mathrm{B}} T_{\mathrm{h}}} \Delta h_{\mathrm{M}} \left[m_{\mathrm{M}} D^{\mathrm{a}}_{\mathrm{MM}} \frac{\partial p_{\mathrm{M}}}{\partial T_{\mathrm{e}}} + m_{\mathrm{A}} D^{\mathrm{a}}_{\mathrm{MA}} \frac{\partial p_{\mathrm{A}}}{\partial T_{\mathrm{e}}} + m_{\mathrm{I}} D^{\mathrm{a}}_{\mathrm{MI}} \frac{\partial p_{\mathrm{I}}}{\partial T_{\mathrm{e}}} + m_{\mathrm{D}} D^{\mathrm{a}}_{\mathrm{MD}} \frac{\partial p_{\mathrm{D}}}{\partial T_{\mathrm{e}}} + \frac{m_{\mathrm{e}}}{\theta} D^{\mathrm{a}}_{\mathrm{Me}} \frac{\partial p_{\mathrm{e}}}{\partial T_{\mathrm{e}}} \right] \\ & + \frac{n}{\rho k_{\mathrm{B}} T_{\mathrm{h}}} \Delta h_{\mathrm{A}} \left[m_{\mathrm{M}} D^{\mathrm{a}}_{\mathrm{AM}} \frac{\partial p_{\mathrm{M}}}{\partial T_{\mathrm{e}}} + m_{\mathrm{A}} D^{\mathrm{a}}_{\mathrm{AA}} \frac{\partial p_{A}}{\partial T_{\mathrm{e}}} + m_{\mathrm{I}} D^{\mathrm{a}}_{\mathrm{AI}} \frac{\partial p_{\mathrm{I}}}{\partial T_{\mathrm{e}}} + m_{\mathrm{D}} D^{\mathrm{a}}_{\mathrm{AD}} \frac{\partial p_{\mathrm{D}}}{\partial T_{\mathrm{e}}} + \frac{m_{\mathrm{e}}}{\theta} D^{\mathrm{a}}_{\mathrm{Ae}} \frac{\partial p_{\mathrm{e}}}{\partial T_{\mathrm{e}}} \right] \\ & + \frac{n}{\rho k_{\mathrm{B}} T_{\mathrm{h}}} \Delta h_{\mathrm{D}} \left[m_{\mathrm{M}} D^{\mathrm{a}}_{\mathrm{DM}} \frac{\partial p_{\mathrm{M}}}{\partial T_{\mathrm{e}}} + m_{\mathrm{A}} D^{\mathrm{a}}_{\mathrm{DA}} \frac{\partial p_{\mathrm{A}}}{\partial T_{\mathrm{e}}} + m_{\mathrm{I}} D^{\mathrm{a}}_{\mathrm{DI}} \frac{\partial p_{\mathrm{I}}}{\partial T_{\mathrm{e}}} + m_{\mathrm{D}} D^{\mathrm{a}}_{\mathrm{DD}} \frac{\partial p_{\mathrm{D}}}{\partial T_{\mathrm{e}}} + \frac{m_{\mathrm{e}}}{\theta} D^{\mathrm{a}}_{\mathrm{De}} \frac{\partial p_{\mathrm{e}}}{\partial T_{\mathrm{e}}} \right] \end{aligned} \tag{33}$$

and

$$\begin{aligned} k_{\mathrm{rh}} = & \frac{n}{\rho k_{\mathrm{B}} T_{\mathrm{h}}} \Delta h_{\mathrm{M}} \left[m_{\mathrm{M}} D^{\mathrm{a}}_{\mathrm{MM}} \frac{\partial p_{\mathrm{M}}}{\partial T_{\mathrm{h}}} + m_{\mathrm{A}} D^{\mathrm{a}}_{\mathrm{MA}} \frac{\partial p_{\mathrm{A}}}{\partial T_{\mathrm{h}}} + m_{\mathrm{I}} D^{\mathrm{a}}_{\mathrm{MI}} \frac{\partial p_{\mathrm{I}}}{\partial T_{\mathrm{h}}} + m_{\mathrm{D}} D^{\mathrm{a}}_{\mathrm{MD}} \frac{\partial p_{\mathrm{D}}}{\partial T_{\mathrm{h}}} + \frac{m_{\mathrm{e}}}{\theta} D^{\mathrm{a}}_{\mathrm{Me}} \frac{\partial p_{\mathrm{e}}}{\partial T_{\mathrm{h}}} \right] \\ & + \frac{n}{\rho k_{\mathrm{B}} T_{\mathrm{h}}} \Delta h_{\mathrm{A}} \left[m_{\mathrm{M}} D^{\mathrm{a}}_{\mathrm{AM}} \frac{\partial p_{\mathrm{M}}}{\partial T_{\mathrm{h}}} + m_{\mathrm{A}} D^{\mathrm{a}}_{\mathrm{AA}} \frac{\partial p_{\mathrm{A}}}{\partial T_{\mathrm{h}}} + m_{\mathrm{I}} D^{\mathrm{a}}_{\mathrm{AI}} \frac{\partial p_{\mathrm{I}}}{\partial T_{\mathrm{h}}} + m_{\mathrm{D}} D^{\mathrm{a}}_{\mathrm{AD}} \frac{\partial p_{\mathrm{D}}}{\partial T_{\mathrm{h}}} + \frac{m_{\mathrm{e}}}{\theta} D^{\mathrm{a}}_{\mathrm{Ae}} \frac{\partial p_{\mathrm{e}}}{\partial T_{\mathrm{h}}} \right] \\ & + \frac{n}{\rho k_{\mathrm{B}} T_{\mathrm{h}}} \Delta h_{\mathrm{D}} \left[m_{\mathrm{M}} D^{\mathrm{a}}_{\mathrm{DM}} \frac{\partial p_{\mathrm{M}}}{\partial T_{\mathrm{h}}} + m_{\mathrm{A}} D^{\mathrm{a}}_{\mathrm{DA}} \frac{\partial p_{\mathrm{A}}}{\partial T_{\mathrm{h}}} + m_{\mathrm{I}} D^{\mathrm{a}}_{\mathrm{DI}} \frac{\partial p_{\mathrm{I}}}{\partial T_{\mathrm{h}}} + m_{\mathrm{D}} D^{\mathrm{a}}_{\mathrm{DD}} \frac{\partial p_{\mathrm{D}}}{\partial T_{\mathrm{h}}} + \frac{m_{\mathrm{e}}}{\theta} D^{\mathrm{a}}_{\mathrm{De}} \frac{\partial p_{\mathrm{e}}}{\partial T_{\mathrm{h}}} \right] \end{aligned} \tag{34}$$

are reactive thermal conductivities of electrons and heavy particles respectively. It should be noted that each of the two reactive conductivities defined above involve all species present. However, they are named after electrons and heavy particles because in the fluid dynamic equations, the first one appears in the electron energy equation and is associated with ∇T_{e}, while the second one appears in the heavy particle energy equation and is associated with ∇T_{h}. The reactive thermal conductivities are finally computed after evaluating the derivatives employing Eqs. (4)–(6).

Chemical and Thermal Non-equilibrium

Under chemical non-equilibrium, conservation of the number density of species 'k' inside a plasma control volume reads as [28]:

$$\frac{\partial n_{\mathrm{k}}}{\partial t} + \nabla \cdot (n_{\mathrm{k}} \vec{u}) + \nabla \cdot \vec{g}_{\mathrm{k}} = \dot{n}_{\mathrm{k}} \tag{35}$$

$n_{\mathrm{k}} \vec{u}$ is the convective flux and g_{k} is the diffusive flux of species 'k'. The diffusive flux can be written as [36] :

$$g_{\mathrm{k}} = \frac{n^2}{\rho} \sum_{j=1}^{v} m_{\mathrm{j}} D^{\mathrm{a}}_{\mathrm{kj}} \left[\nabla x_{\mathrm{j}} + (x_{\mathrm{j}} - \frac{\rho_{\mathrm{j}}}{\rho}) \nabla \ln p \right] - \frac{n}{\rho} \sum_{j=1}^{v} \left(\frac{n_{\mathrm{j}} Z_{\mathrm{j}} e D_{\mathrm{kj}}}{kT} \right) E^{\mathrm{X}} - \frac{D^{\mathrm{aT}}_{\mathrm{k}}}{m_{\mathrm{k}}} \nabla \ln T_{\mathrm{k}} \tag{36}$$

E^{X} is the external electric field.

Equation (35) can be interpreted as a modified Saha equation including the effect of chemical non-equilibrium. To emphasize this fact we take the example of single ions for which the right side of Eq. (35) appears as [28]:

$$\dot{n}_{\mathrm{I}} = \alpha_{\mathrm{I}} n_{\mathrm{a}} \left[S_2 - \frac{n_{\mathrm{e}} n_{\mathrm{I}}}{n_{\mathrm{a}}} \right] \tag{37}$$

S_2 is the equilibrium rate constant of reaction-2 and α_{I} is the recombination coefficients of ions. Equation (35) can now be written in the form:

$$\frac{\partial n_{\mathrm{I}}}{\partial t} + \nabla \cdot (n_{\mathrm{I}} \vec{u}) + \nabla \cdot \vec{g}_{\mathrm{I}} = \alpha_{\mathrm{I}} n_{\mathrm{a}} [S_2 - n_{\mathrm{e}} n_{\mathrm{I}} / n_{\mathrm{a}}]$$

Rearrangement of the terms results in:

$$\frac{n_{\mathrm{e}} n_{\mathrm{I}}}{n_{\mathrm{a}}} = R_2 = S_2 - \Delta S_2 \tag{38}$$

We call this as modified Saha equation for first ionization that takes chemical non-equilibrium into account. R_2 is the ultimate rate constant for reaction-2 (atom to ion formation) obtained through a modification of the equilibrium rate constant S_2 by chemical non-equilibrium contribution ΔS_2.

$$\Delta S_2 = \frac{1}{\alpha_I n_{\mathrm{a}}} [\nabla.(n_{\mathrm{I}} \vec{u}) + \nabla \cdot \vec{g}_{\mathrm{I}}] \tag{39}$$

Similar rate constants R_{i}, equilibrium rates S_{i} and corresponding non-equilibrium contributions ΔS_{i} can be obtained for i^{th} associated reaction.

We now introduce the chemical non-equilibrium parameter 'r_{i}' for the ith associated reaction as the ratio:

$$r_i = \frac{S_{\mathrm{i}} - \Delta S_{\mathrm{i}}}{S_i} \tag{40}$$

Similar to the temperature non-equilibrium parameter θ, r_{i} can now identify the exact effect of existing chemical non-equilibrium for the ith reaction. Results are presented estimating such effects at different pressures and thermal non-equilibria.

Results

Using the above method of computation, results obtained are presented in the following. Particular θ values: 1, 2, 3, 5, 10, 20 and 30 are chosen judiciously to maintain clarity of presentation and ranges of interest. Chosen pressure values for presentation are 0.1, 1.0, 4.0 and 7.0 atmospheres. Selected higher and lower pressure ranges are close to respectively upstream and downstream pressures inside of arc plasma torches. Although, value of effective rate constant may exceed corresponding equilibrium rate constant by orders of magnitude depending on plasma condition and geometry, values of 'r' in the present computation are chosen to range from 0.5 to 2. This is based on a non-equilibrium modeling study of an oxygen cutting torch (2 mm nozzle diameter) where

'r' for dominant reactions are found to range from 0.7 to 1.5 within the computational domain. Results of chemical non-equilibria are presented accordingly. Overall property behavior differs from that in monatomic gases mainly due to the presence of dissociative reactions at lower heavy species temperatures. Thermodynamic properties are presented first. Results of transport properties are presented subsequently starting with a comparison with published results under equilibrium. Unless otherwise specified, the numbers associated with each curve in the presented results indicate corresponding θ values. All results presented up to Fig. 15 assume r_i=1 for all reactions. In an effort to illustrate the possible effects of the chemical-non-equilibrium ($r_i \neq 1$) on the properties, the graphs [Figs. 16–19] are presented with $r_1 = r_2 = r_3 = r$, where r varies from 0.5 to 2. It must be emphasized that the three non-equilibrium parameters (r_1, r_2 and r_3) are very likely to differ from each other in most of the cases. The parameters are chosen equal just to limit the number of graphs in the presentations. Possible formations of negative ions due to attachment of electrons are completely neglected in the present computation in all cases. At lower pressure ($\leq$ 1atm) presence of O^{3+} may significantly influence the property at temperatures beyond 40,000 K due to enhanced Coulomb cross-section of O^{3+}. While the computed results for higher pressures may be reasonably accurate, at lower pressure, due to omission of O^{3+}, they may be inaccurate by more that 5% for temperatures above about 45,000 K for 1 atm and for temperatures above about 40,000 K for 0.1 atm.

Variation of the number density of various species as a function of temperature for different θ values is presented in Fig. 1. Figure 2 shows the variation of the total number

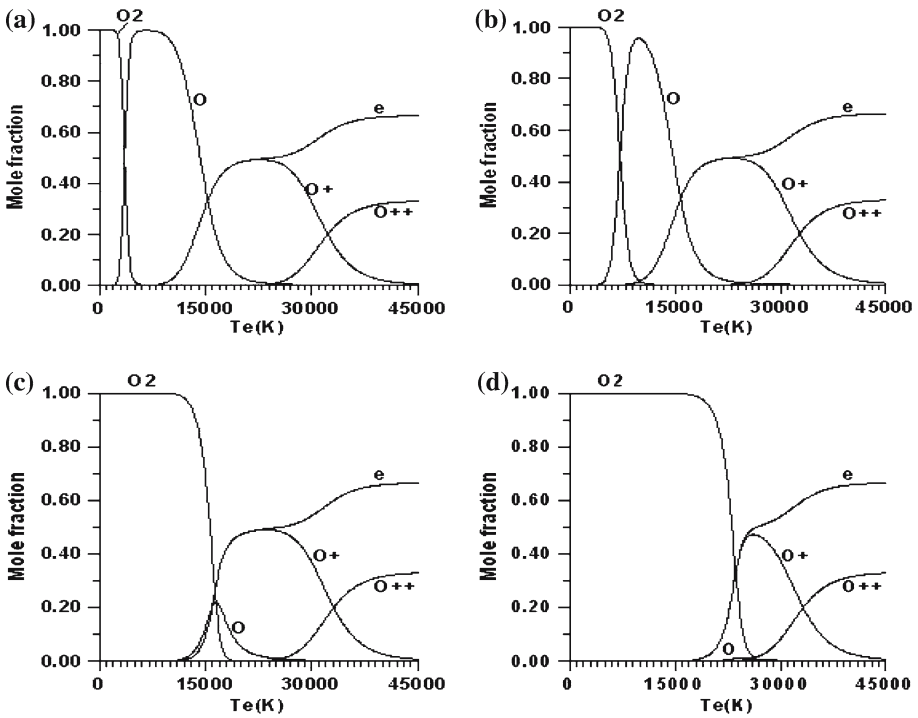

Fig. 1 Molefraction of different species in oxygen plasmas under different degrees of non-equilibrium at atmospheric pressure: (**a**) T_e/T_h = 1, (**b**) T_e/T_h = 2, (**c**) T_e/T_h = 5, (**d**) T_e/T_h = 10

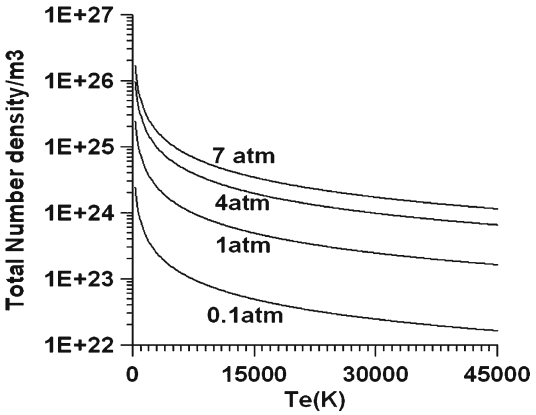

Fig. 2 Variation of total number density as a function of temperature with pressure as parameter

density as a function of pressure. Although individual species number densities depend on θ, the total number density is independent of it and depends only on the total pressure. Individual number densities of species can be identified using the mole fraction result of Fig. 1 together with Fig. 2. The atom density shows an interesting behavior for larger values of θ. As soon as a molecule is dissociated, the atoms will be immediately ionized

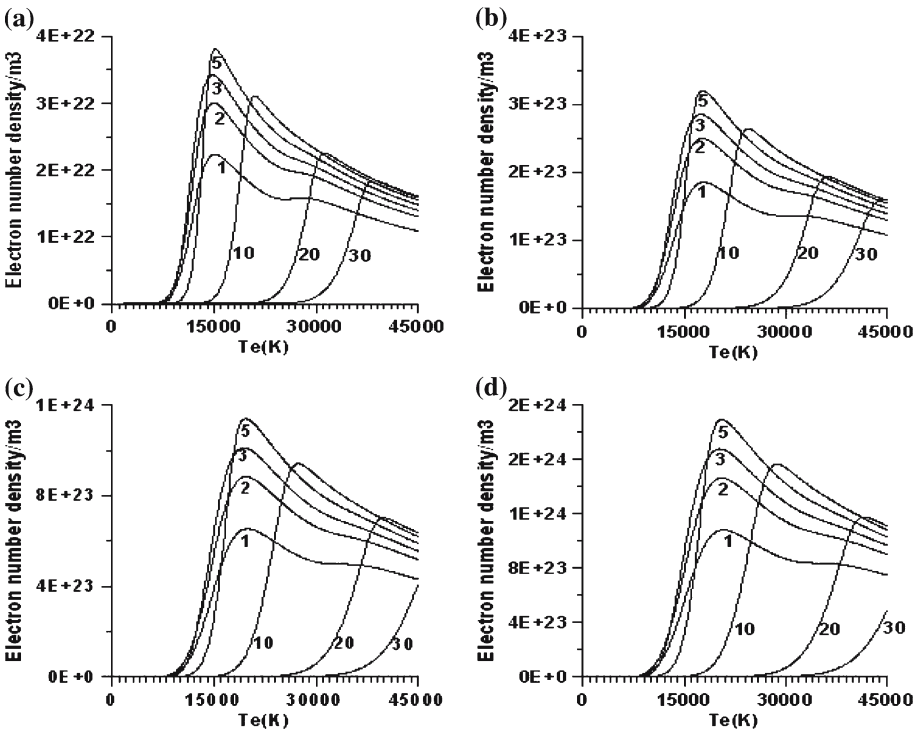

Fig. 3 Electron number density: (**a**) 0.1 atmosphere, (**b**) 1 atmosphere, (**c**) 4 atmospheres, (**d**) 7 atmospheres. Number associated with each curve indicates T_e/T_h ratio

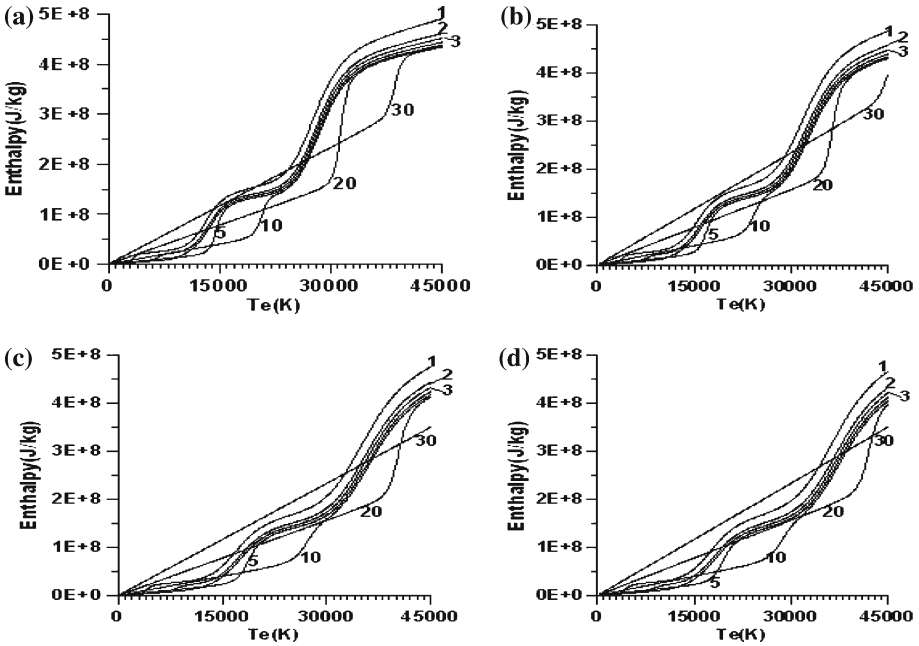

Fig. 4 Total enthalpy variation: (**a**) 0.1 atmosphere, (**b**) 1 atmosphere, (**c**) 4 atmospheres, (**d**) 7 atmospheres. Number associated with each curve indicates T_e/T_h ratio

because of the high electron temperature. As a consequence, the atom density almost vanishes for higher values of θ. Figure 3 presents variations of electron number density with p, T_e and θ. Although, there is a strong dependence of the total number density on pressure, the trend of variation with θ remains almost identical. It can be noted that the peak in number density occurs around T_e equal to 15,000K for θ up to around 5 and then the peak decreases and also shifts in position towards higher T_e. For $\theta > 5$ and T_e around 15,000 K, T_h will be below the dissociation temperature and the electron number density (n_e) becomes very small, because there is almost no dissociation and therefore, no ionization. For $\theta \geq 10$, the peaks of n_e shift to higher values of T_e, because dissociation and hence ionization are delayed until $T_h(= T_e/10)$ reaches dissociation temperature. Dissociation of molecules serves as the root cause for the generation of every other species present in the system.

Figure 4 presents variation of total enthalpy as a function of electron temperature for various values of θ. It is almost linear with T_e unless some reactions like dissociation or ionization occur at certain temperatures. Similar to earlier observations, the behavior for higher θ are distinctly different from behavior at lower θ caused by similar reasons. Except a drift of the curves toward higher T_e, the overall variation in enthalpy with change of pressure is small. Specific heat at constant pressure (c_p) for electrons and heavy particles are derived from the respective enthalpy component behavior with respect to T_e and T_h and presented in Figs. 5 and 6 respectively. Particular variation of the number density with temperature for a given θ contributes towards the height of the peaks observed.

Figure 7 compares our results for transport properties obtained under chemical and thermal equilibrium with those already published in the literature. While overall agreement is good, excellent agreement is observed for viscosity and slight deviations are observed

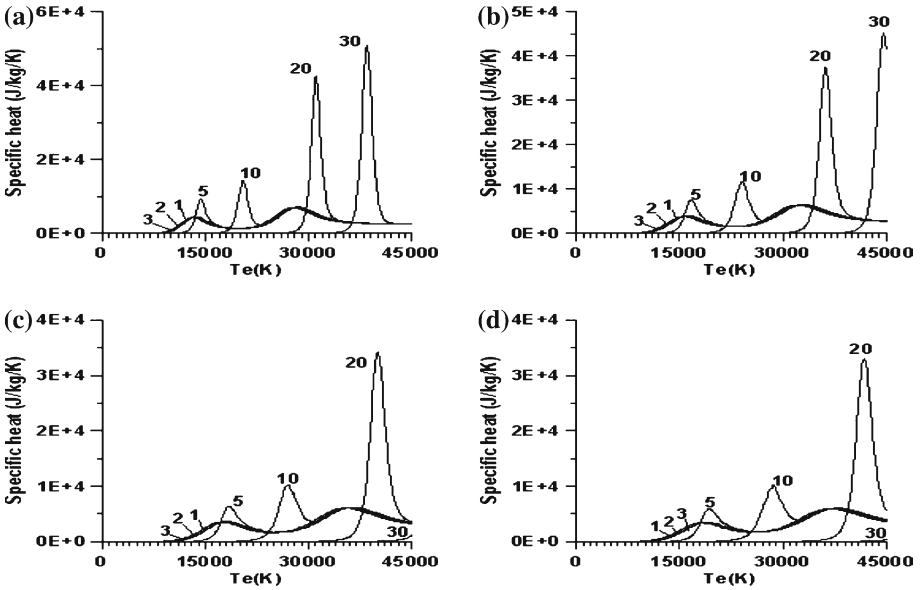

Fig. 5 Variation of specific heat of electrons as a function of temperature: (**a**) 0.1 atmosphere, (**b**) 1 atmospheres, (**c**) 4 atmospheres, (**d**) 7 atmospheres. Number associated with each curve indicates T_e/T_h ratio

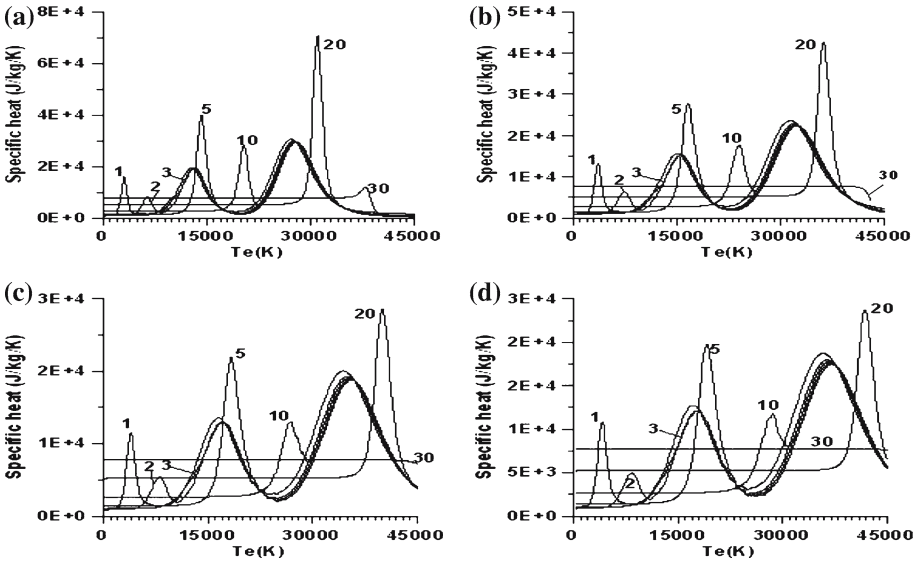

Fig. 6 Variation of specific heat of heavy particles as a function of temperature: (**a**) 0.1 atmosphere (**b**) 1 atmosphere, (**c**) 4 atmospheres, (**d**) 7 atmospheres. Number associated with each curve indicates T_e/T_h ratio

for thermal conductivity and electrical conductivity. The variations may be attributed to the use of different sets of collision integrals and difference in the formulations used. It may be noted that the differences in the reactive thermal conductivity between the present results

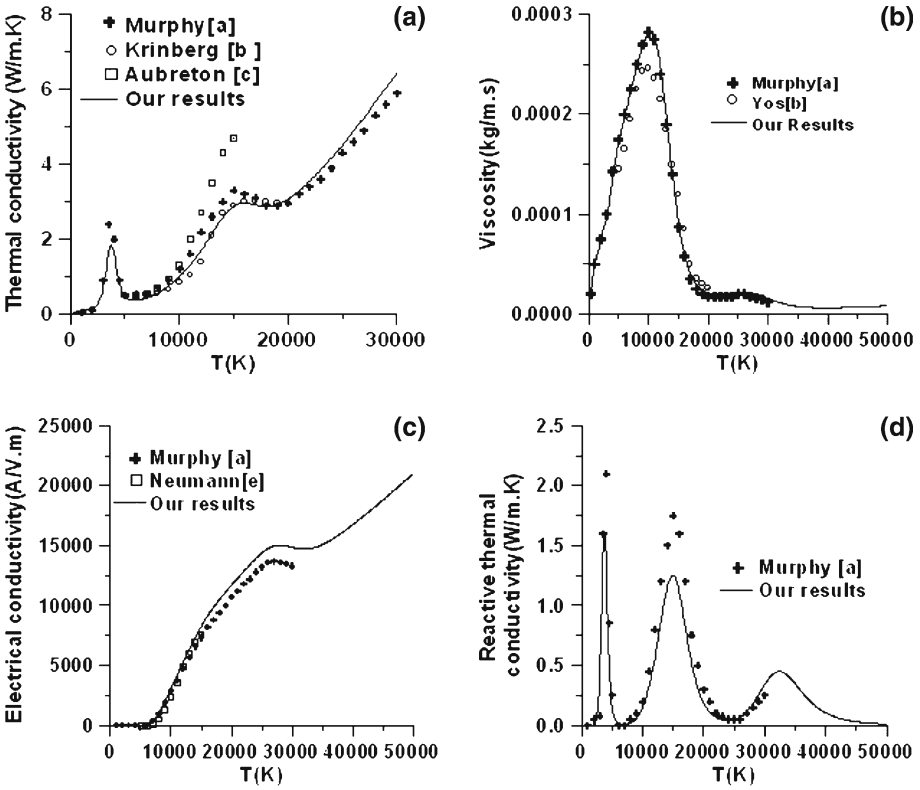

Fig. 7 Comparison of transport properties of atmospheric pressure equilibrium oxygen plasma, obtained from this study, with previously reported results: (**a**) Total thermal conductivity, (**b**) Viscosity, (**c**) electrical conductivity, (**d**) Reactive thermal conductivity: [a]—Ref. [3]; [b]—Ref. [39]; [c]—Ref. [16]; [d]—Ref. [40]; [e]—Ref. [41]

and those of Murphy (Fig. 7d) seem to be due to the different formulations used to calculate this property (that of Kannappan and Bose here, and that of Butler and Brokaw by Murphy), since both the current work and Murphy use the same O–O and O–O^+ collision integrals.

Various components of the total thermal conductivity of Fig. 7(a) are presented in Fig. 8. Figures 9 and 10 present the translational thermal conductivities of electrons and heavy particles respectively for various θ and pressure values. Once the dissociation temperature has been reached, the thermal conductivity of electrons swiftly approaches the curve followed by lower θ values. Availability of higher number density of particles at higher pressure increases the magnitude of the thermal conductivity for both electrons and heavy particles.

The electrical conductivity is a property of electrons alone and its variation with electron temperature is presented in Fig. 11. For higher pressures, it exhibits higher values due to higher number densities. With higher θ values, the electrical conductivity starts rising fast once the dissociation temperature has been reached and then quickly stabilizes near the values observed for lower values of θ at that T_e.

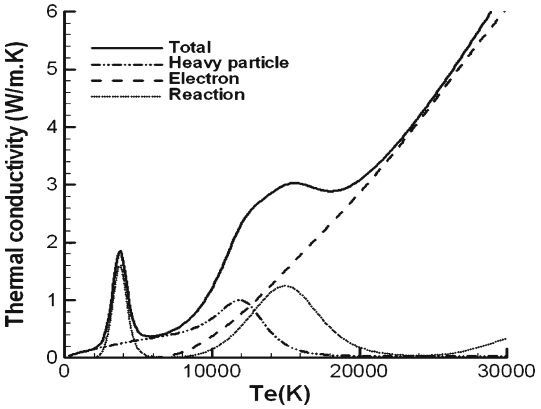

Fig. 8 Components of the thermal conductivity of oxygen presented in Fig.7(**a**)

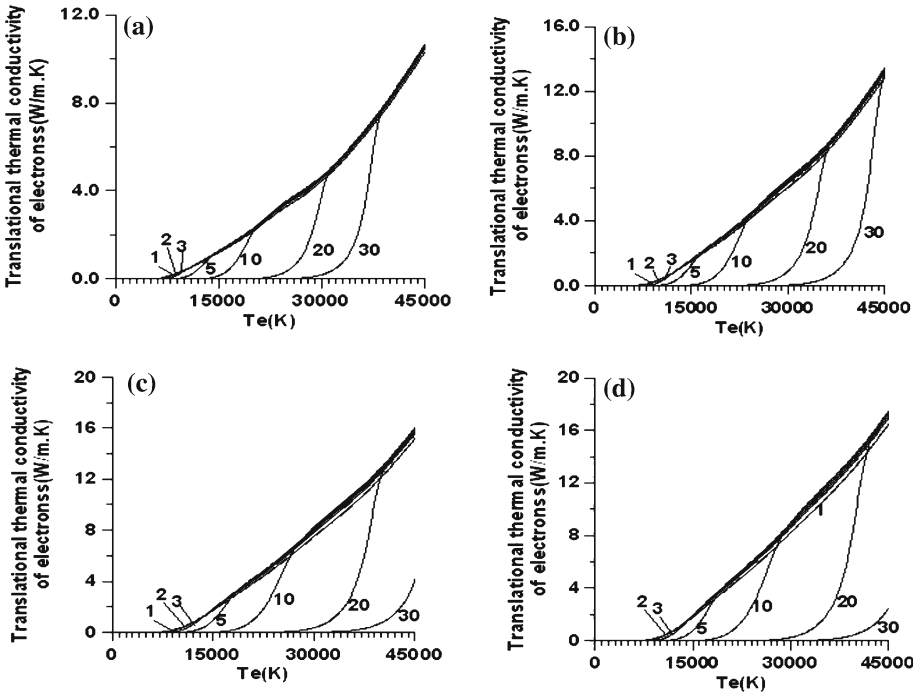

Fig. 9 Translational thermal conductivity of electrons: (**a**) 0.1 atmosphere, (**b**) 1 atmosphere, (**c**) 4 atmospheres, (**d**) 7 atmospheres. Number associated with each curve indicates T_e/T_h ratio

The reactive thermal conductivity of electrons and heavy particles are presented in Figs. 12 and 13 respectively. While for electrons the peaks are observed at first and second ionization, for heavy particles the peaks appear at the molecular dissociation temperature. The reactive thermal conductivity basically depends on the variation of the number density of particles with associated temperature [Eqs. (33)–(34)]. Sharper variations in the number density with T_h at higher θ for heavy particles result in the gradually increasing size of the peaks with θ for the heavy particle thermal conductivity.

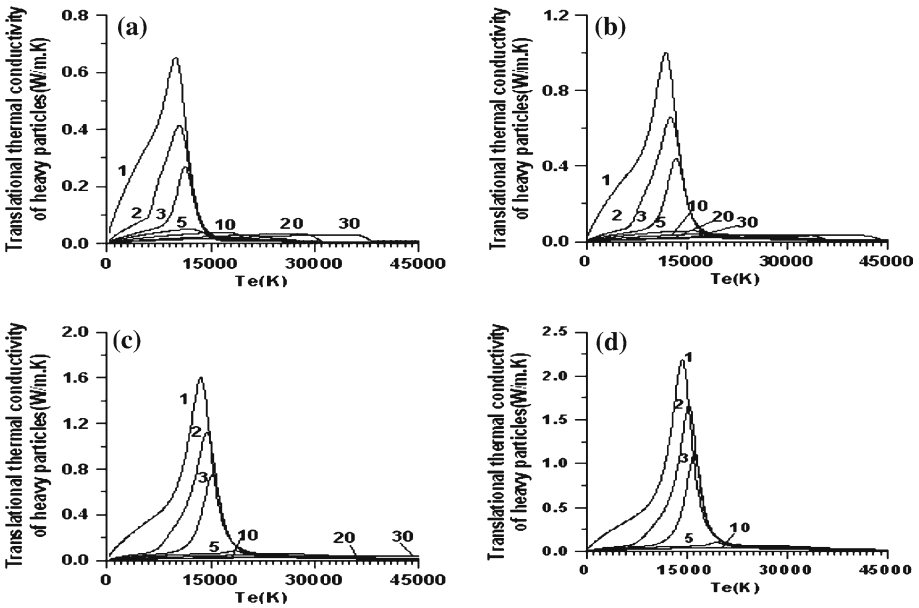

Fig. 10 Translational thermal conductivity of heavy particles (**a**) 0. 1 atmosphere, (**b**) 1 atmosphere, (**c**) 4 atmospheres, (**d**) 7 atmospheres. Number associated with each curve indicates T_e/T_h ratio

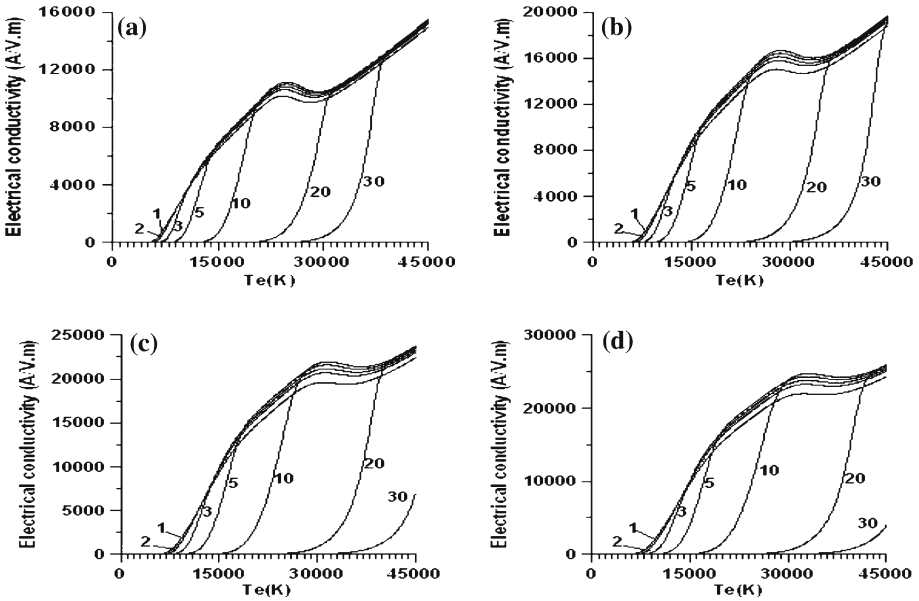

Fig. 11 Electrical conductivity: (**a**) 0.1 atmosphere, (**b**) 1 atmosphere, (**c**) 4 atmospheres, (**d**) 7 atmospheres. Number associated with each curve indicates T_e/T_h ratio

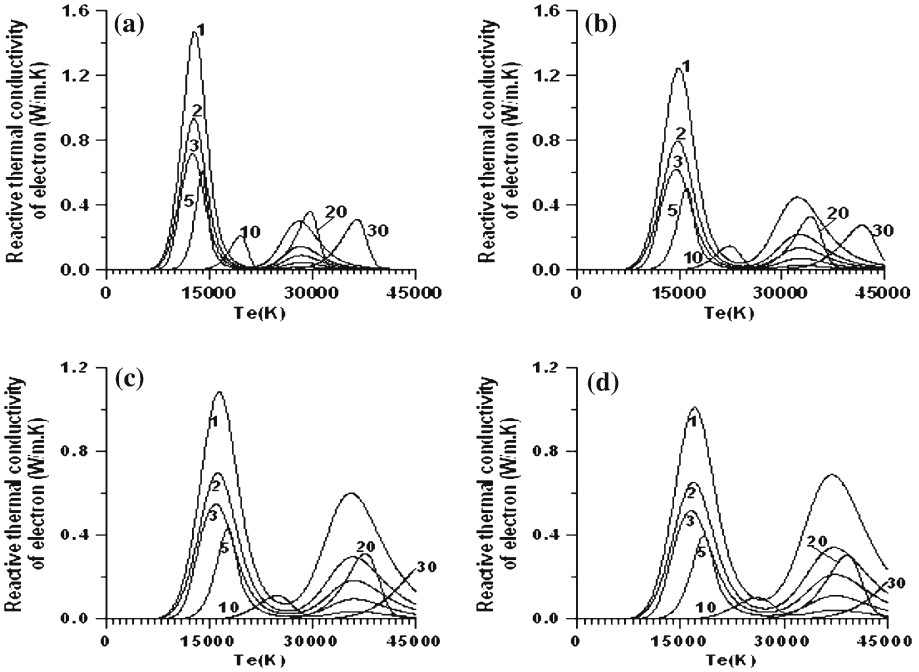

Fig. 12 Reactive thermal conductivity of electrons: (**a**) 0.1 atmosphere, (**b**) 1 atmosphere, (**c**) 4 atmospheres, (**d**) 7 atmospheres. Number associated with each curve indicates T_e/T_h ratio

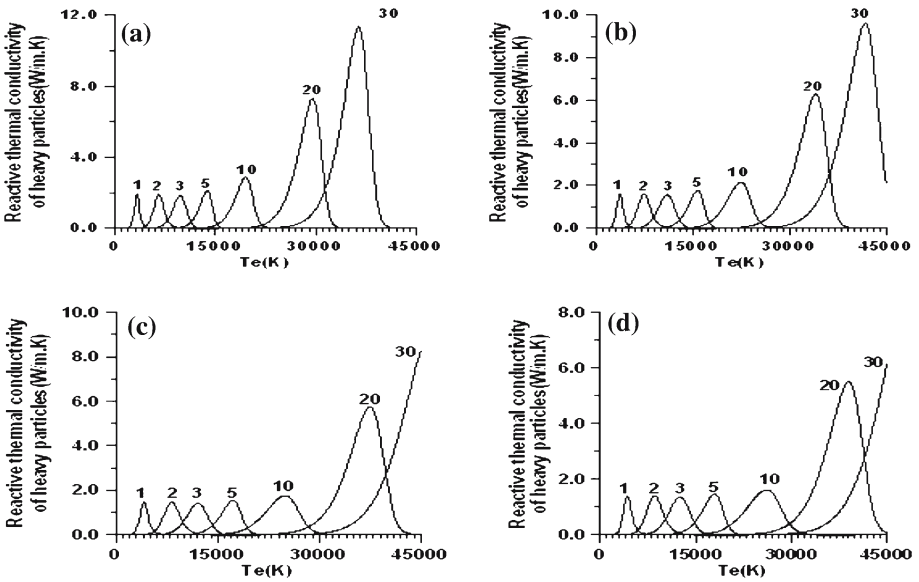

Fig. 13 Reactive thermal conductivity of heavy particles: (**a**) 0.1 atmosphere, (**b**) 1 atmosphere, (**c**) 4 atmospheres, (**d**) 7 atmospheres. Number associated with each curve indicates T_e/T_h ratio

Figure 14 presents variations of viscosity with pressure, temperature and θ. It is the momentum transport, responsible for viscosity of a gas. Viscosity of a gas increases till ionization starts due to increase in gas particle velocities with temperature. However, once ionization starts, long-range coulomb interaction increases with enhanced ionization and results in the observed drop in the viscosity value. Viscosity is primarily a property of the heavy particles. For a given T_e, if θ increases, T_h decreases, resulting in a drop in the momentum transport and hence a drop in the viscosity value. With increasing θ, the peaks in the viscosity shift towards higher T_e values. The viscosity increases with increasing pressure.

Volumetric collision frequencies between electrons and heavy particles are presented in Fig. 15. Decrease in collision frequency with electron temperature is primarily caused by a decrease in number density of electrons with temperature. The shift of the peaks can be explained again by the behavior of the dissociation temperature for a given θ.

In Figs. 16–19, we have presented the effect of chemical non-equilibrium on various properties. The total thermal conductivity, the electrical conductivity and the viscosity in addition to the enthalpy have been chosen for this study. The chemical non-equilibrium parameters in these figures are assumed to be equal for all reactions: $r_1 = r_2 = r_3 = r$. $r = 1$ corresponds to chemical equilibrium. Figures 16 and 17 present results at pressures of 1 and 7 atmospheres respectively for $\theta = 1$. It is observed that at lower temperatures, deviations due to chemical non-equilibrium are relatively small. However, at higher temperatures, these deviations are appreciable. A similar scenario is observed in the properties presented in Figs. 18 and Fig. 19 for $\theta = 5$ and similar pressures. The effects of variations due to θ are somewhat more pronounced for the viscosity.

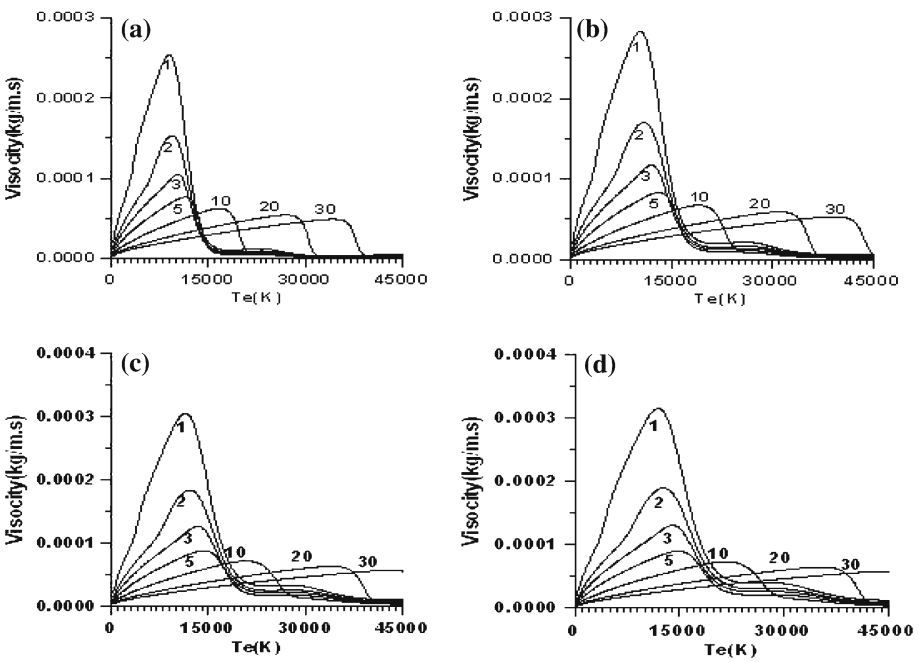

Fig. 14 Viscosity (**a**) 0.1 atmosphere, (**b**) 1 atmosphere, (**c**) 4 atmospheres, (**d**) 7 atmospheres. Number associated with each curve indicates T_e/T_h ratio

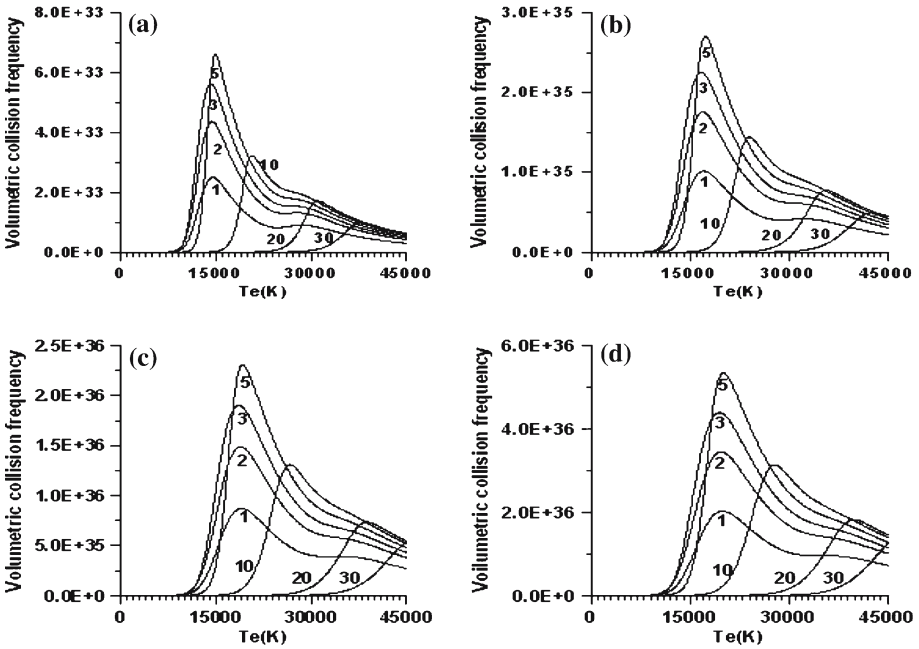

Fig. 15 Volumetric collision frequency: (**a**) 0.1 atmosphere, (**b**) 1 atmosphere, (**c**) 4 atmospheres, (**d**) 7 atmospheres. Number associated with each curve indicates T_e/T_h ratio

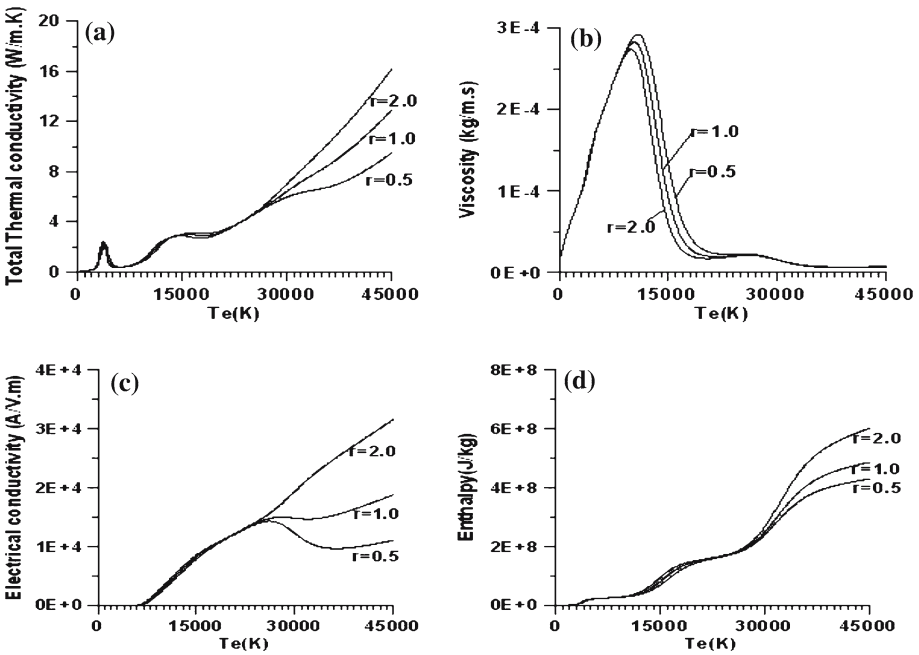

Fig. 16 Effect of chemical non-equilibrium on transport and thermodynamic properties at p = 1 atm and T_e/T_h=1: (**a**) Total thermal conductivity, (**b**) Viscosity, (**c**) Electrical conductivity, (**d**) Enthalpy

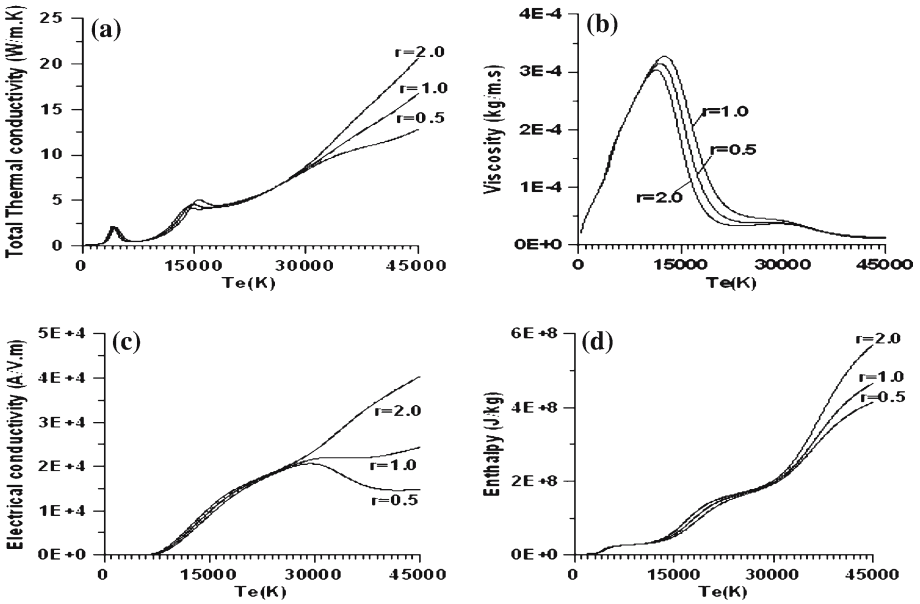

Fig. 17 Effect of chemical non-equilibrium on transport and thermodynamic properties at p = 7 atm and T_e/T_h = 1: (**a**) Total thermal conductivity, (**b**) Viscosity, (**c**) Electrical conductivity, (**d**) Enthalpy

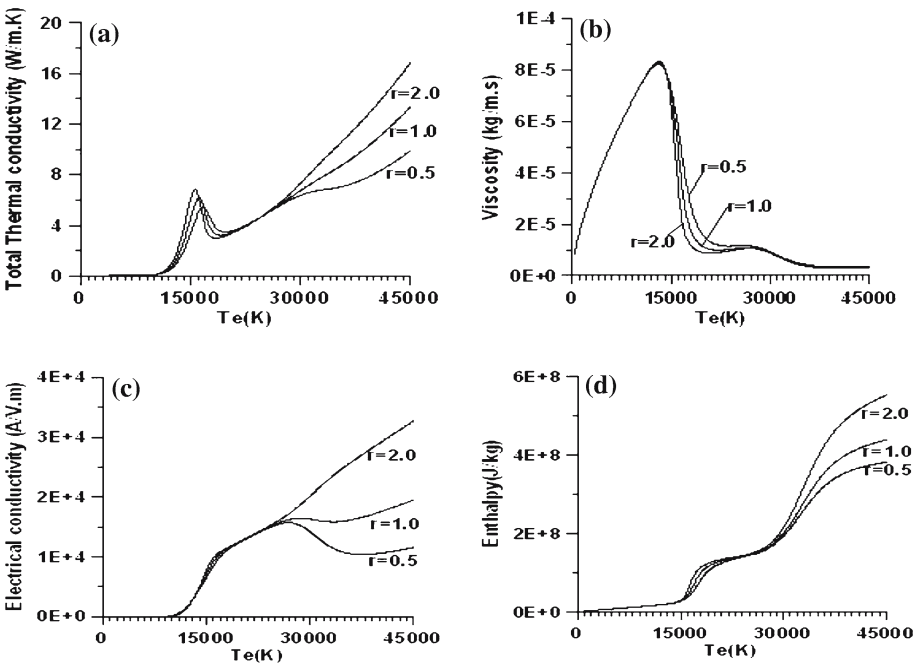

Fig. 18 Effect of chemical non-equilibrium on transport and thermodynamic properties at p = 1 atm and T_e/T_h = 5: (**a**) Total thermal conductivity, (**b**) Viscosity, (**c**) Electrical conductivity, (**d**) Enthalpy

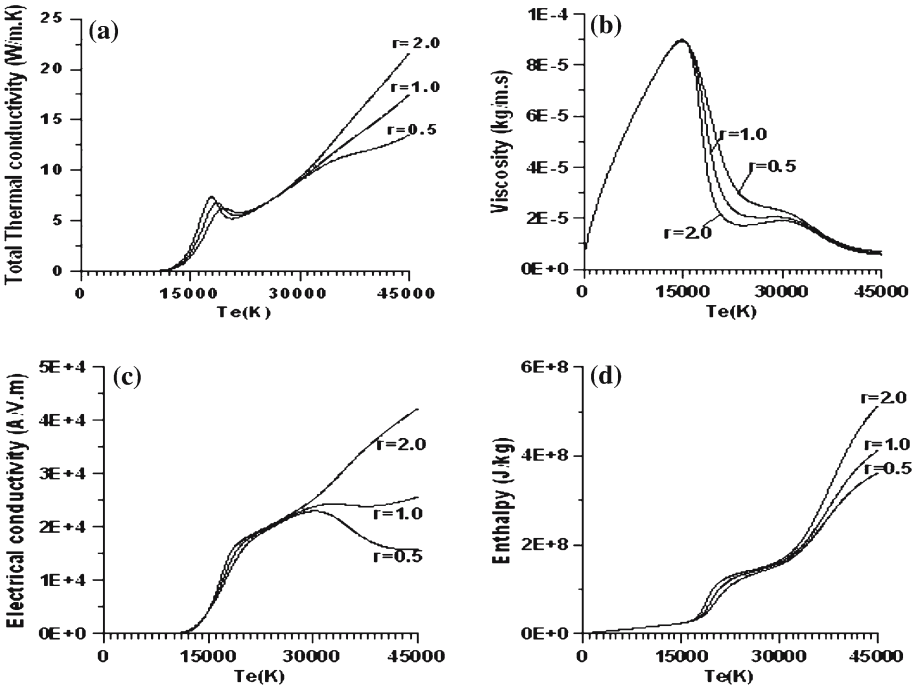

Fig. 19 Effect of chemical non-equilibrium on transport and thermodynamic properties at p = 7 atm and T_e/T_h = 5: (**a**) Total thermal conductivity, (**b**) Viscosity, (**c**) Electrical conductivity, (**d**) Enthalpy

Summary And Conclusions

In this paper, values for thermodynamic and transport properties are presented for an oxygen plasma under non-equilibrium conditions. The non-equilibrium properties have been calculated for the conditions of a two-temperature plasma, with an electron temperature different from that of the heavy species temperature, and for a plasma where there is in addition a deviation from composition equilibrium due to diffusion or delayed recombination effects. The property values are given for a range of pressures of 0.1 to 7 atm, and for a range of electron temperatures from 300 K to 45,000 K. This range is wider than the ranges usually found in the literature because it was found necessary to provide values for CFD calculations where there may be an oscillatory behavior of the solution before convergence. The non-equilibrium considered is expressed as the ratio θ of electron temperature to heavy species temperature, and of the ratio r of a species actual density derived from kinetic calculations and that derived for equilibrium at T_e. These non-equilibrium parameters have been varied from $1 < \theta < 30$ and $0.5 < r < 2$. This range of chemical composition non-equilibrium covers most of the situations encountered in practice, in particular if one considers that higher θ values frequently accompany diffusion effects, thus reducing the value of r that is observed. While it has been observed that θ has a strong influence on all the properties over a wide range of temperatures, chemical composition non-equilibrium is found to significantly influence the properties only at higher values of electron temperature. The fact that for appropriate values of θ dissociation reactions may co-exist with ionization reactions at high T_e plays a key role in influencing

the property values. This is particularly noticeable in the values for the non-equilibrium specific heats and for the reactive thermal conductivity. Under chemical composition non-equilibrium conditions, the production rates of various species are modified by particle fluxes due to density gradients, and this effect can ultimately be reduced to the use of modified rate constants in the associated rate equations. Results of calculations for $\theta = 1$ and $r = 1$ represent equilibrium values of the properties, and the data obtained for these conditions compare favorably with those published previously.

Acknowledgements The authors would like to thank Hypertherm Inc. for financial support. One of the authors (S. Ghorui) is thankful to Department of Atomic Energy, India for grant of leave for post-doctoral study.

References

1. Devoto RS (1967) Phys Fluids 10:354
2. Devoto RS (1973) Phys Fluids 16:616
3. Murphy AB, Arundell CJ (1994) Plasma Chem Plasma Process 14:451
4. Murphy AB (1995) Plasma Chem Plasma Process 15:279
5. Murphy AB (1997) IEEE Trans Plas Sci 25:809
6. Murphy AB (2000) Plasma Chem Plasma Process 20:279
7. Fauchais P, Elchinger MF, Aubreton J (2000) J High Temp Material Process 4:21
8. Aubreton J, Elchinger MF, Fauchais P, Rat V, Andre P (2004) J Phys D Appl Phys 37:2232
9. Hirschfelder JO, Kurtis CF, Bird RB (1964) Molecular theory of gases and liquids, 2nd edn. Wiley, New York
10. Chapman S, Cowling TG (1972) The mathematical theory of transport processes in gases. North-Holland, Amsterdam
11. Devoto RS (1967) Phys Fluids 10:2105
12. Devoto RS (1965) Ph.D. thesis, Stanford University
13. Miller EJ, Sandler SI (1973) Phys Fluids 16:491
14. Kannappan D, Bose TK (1977) Phys Fluids 20:1668
15. Bonnefoi C (1983) State thesis, University of Limoges, France
16. Aubreton J, Bonnefoi C, Mexmain JM (1986) Rev Phys Appl 21:365
17. Rat V, Andre P, Aubreton J, Elchinger MF, Fauchais P, Lefort A (2001) Phys Rev E 64:064091
18. Rat V, Aubreton J, Elchinger MF, Fauchais P (2001) Plasma Chem Plasma Process 21:355
19. Rat V, Andre P, Aubreton J, Elchinger MF, Fauchais P, Lefort A (2002) Plasma Chem Plasma Process 22:453
20. Rat V, Andre P, Aubreton J, Elchinger MF, Fauchais P, Lefort A (2002) Plasma Chem Plasma Process 22:475
21. Rat V, Andre P, Aubreton J, Elchinger MF, Fauchais P, Vacher D (2002) J Phys D Appl Phys 35:981
22. Aubreton J, Elchinger MF, Rat V, Fauchais P (2004) J Phys D Appl Phys 37:34
23. Ramshaw JD (1993) J Non-Equilib Thermodyn 18:121
24. Ramshaw JD (1996) J Non-Equilib Thermodyn 21:233
25. Andre P, Aubreton J, Elchinger MF, Rat V, Fauchais P, Lefort A, Murphy AB (2004) Plasma Chem Plasma Process 24:435
26. Chen X, Han P (1999) J Phys D Appl Phys 32:1711
27. van de Sanden MCM, Schram PPJM, Peeters AG, van der Mullen JAM, Kroesen GMW (1989) Phys Rev A 40:5273
28. Mitchner M, Kruger CH (1973) Partially ionized gases. Wiley, New York
29. Ferziger JH, Kaper HG (1972) Mathetical theory of transport processes in gases. North Holland, Amsterdam
30. Devoto RS (1966) Phys Fluids 9:1230
31. Levin E, Patridge H, Stallcop JR (1990) J Thermophysics 4:469
32. Yun KS, Mason EA (1962) Phys Fluid 5:380
33. Stallcop JR, Patridge H, Levin E (1991) J Chem Phys 95:6429
34. Devoto RS (1976) Phys Fluid 19:22
35. Liboff RI (1959) Phys Fluid 2:40

36. Murphy AB (1993) Phys Rev E 48:3594
37. Li HP, Chen X (2001) Chin Phys Lett 18:547
38. Bose TK, Kannappan D, Seeniraj RV (1985) Warme-und Stoffubertragung 19:3
39. Krinberg IA (1965) High Temp (USSR) 3:606
40. Yos JM (1965) Report RAD TF-65, AVCO Corporation, Wilmington, Massachusetts
41. Neumann W, Sacklowski U (1968) Beitr Plasma Phys 8:57